Biol. Cybern. 79, 309–321 (1998)

Biological Cybernetics
© Springer-Verlag 1998

Statistical model of the hippocampal CA3 region
II. The population framework: model of rhythmic activity in the CA3 slice

G. Barna, T. Grőbler, P. Érdi

Department of Biophysics, KFKI Research Institute for Particle and Nuclear Physics of the Hungarian Academy of Sciences, P.O. Box 49, H-1525 Budapest, Hungary

Received: 29 August 1997 / Accepted in revised form: 17 July 1998

Abstract. A statistical model is given to describe the electrical activity patterns of large neural populations of the hippocampal CA3 region. A continuous model has been formalized to describe the statistical processes governing the interactions within and between neural fields. The system of partial differential equations contains diffusion terms which determine the evolution of second moments of the probability distribution functions. The model is supplemented with a differential description of post-synaptic potentials. The discretization procedure has been designed so as to make the discrete equations scaling invariant.

Population activities as well as underlying single-cell voltages are simulated during normal and epileptiform activities in the hippocampal CA3 slice. It is demonstrated that our model can reproduce electrophysiological phenomena characteristic to both single-cell and population activities. Specifically, fully synchronized population bursts, synchronized synaptic potentials, and low amplitude population oscillation were obtained.

1 Introduction

The complete description of cortical structures using network models composed of morphologically and biophysically detailed single cells is not only extremely difficult, because of the large number of neurons, but also superfluous, since to study the system's behavior we hardly need to know the state of each individual neuron. There is a long tradition to try to connect the 'microscopic' single-cell behavior to the global 'macrostate' of the nervous system, analogously to the procedures applied in statistical physics. Global brain dynamics is handled by using a continuous (neural field) description instead of the networks of discrete nerve cells. Both determinstic, field-theoretical (Beurle 1956; Griffith 1963; Seelen 1968; Wilson and Cowan 1973; Amari 1983) and more statistical approaches (Cowan 1968; Amark 1974; Ingber 1982; Peretto 1984, 1992) have been developed. The determinsitic approach has recently been extended for interacting layers (Mallot and Giannakopoulos 1996) to be more appropriate for modeling cortical networks.

In the deterministic field-theoretical description, each neuron is represented as a point in the neural layer or field and a neuronal density is defined, while the statistical mechanical approach also deals with the state space, and the density functions are extended to all state variables.

In a long series of papers starting from 1974, Ventriglia (1974, 1988, 1990, 1994) constructed a neural kinetic theory of large-scale brain activities. Ventriglia's kinetic theory is a statistical field theory. He assumed two types of entities: spatially fixed neurons and spatialy propagating spikes ('impulses'). In Part I we introduced a much more complex single-cell model than that used by Ventriglia. The response of CA3 pyramidal cells to injected currents, namely intrinsic burst discharges and repetitive firing, were reproduced. This single-cell module is now incorporated into our statistical population framework. Our model (Grőbler and Barna 1996; Érdi et al. 1997; Grőbler and Barna 1997) is a model with diffusion, based on Ventriglia's notion of two entities. Other essential developments and differences are listed in Sect. 2.

In this paper we show that, with the aid of the statistical approach, large-scale hippocampal phenomena can be simulated, while the behavior of an 'average cell' can also be monitored. The role of inhibitory and excitatory interactions is studied. Specifically, phenomena characteristic to the CA3 region, such as fully synchronized population bursts, synchronized synaptic potentials, and low amplitude population oscillation, are reproduced. In addition, simulations have been done for the case of the total suppression of inhibition. Under this condition, synchronized population activity occurs in consequence of the excitatory interactions between pyramidal cells, as comparative experiments and simulations with networks also demonstrate (Traub and

Correspondence to: P. Érdi (e-mail: erdi@rmki.kfki.hu)

Miles 1991, 1992). The occurrence of fully synchronized bursts, and their propagation in space, are also demonstrated here.

2 Basic model properties

The description of the population activity of neurons requires different mathematical apparatus from that of individual neurons. In addition, the statistical approach presented here uses the notion of two separate populations, one for the neurons and the other for action potentials. Thus, for the sake of simplicity, the following expressions will be used throughout the rest of the paper:

- spike emission: action potential generation
- number of emitted spikes: number of synaptic sites that a single action potential can reach
- spike propagation: action potential conduction through the axonal arbor
- spike absorption: arrival of the action potential at a synaptic site and change of postsynaptic membrane conductance
- probability density function (PDF): refers to the number of neurons/spikes that are in a given state at the same time
- diffusion: the effects, not explicit in the model, that make the neurons/spikes get to slightly different states

The model describes neural population activity in terms of the PDFs of (1) neurons and (2) spikes traveling between the neurons. This idea is adopted from earlier work by Ventriglia (1974, 1988, 1994). The state space consists of the two-dimensional space coordinate $\mathbf{r}$ (for both neurons and spikes), a membrane potential coordinate u (for neurons), and an intracellular calcium-concentration coordinate χ (for pyramidal neurons only). The different neural populations s (pyramidal and two types of inhibitory cells) have their own neuronal fields which can interact through the emission and absorption of spikes (action potentials). The neurons are fixed in space while spikes can travel among them.

This description necessarily involves the statistical treatment of synaptic connections between neurons. This is statistically equivalent with the random connectivity used in other CA3 models (e.g. Traub and Miles 1991). The specificity of individual connections [or long-range effects (Ventriglia 1988)], however, should be taken into account in a later version of this model.

A fundamental assumption of the model is that the important aspect of neural information processing is the *number and timing of action potentials* rather than their exact shape that shows little variability. According to this assumption, the firing state of neurons is handled separately, while the sophisticated part of the model describes interspike behavior.

Though the basic idea of the model comes from earlier work by Ventriglia (1974, 1988, 1994), the following essential developments should be emphasized:

- The present model is a *diffusion* model which enables cells that are initially in the same state to be dispersed among different states. Accordingly, the model includes diffusion of neurons over the state space (membrane potential and calcium concentration) and diffusion of spikes in space.
- The single-cell model is based on different *ionic conductances* specific to each cell type.
- An additional variable, the *intracellular calcium concentration* of pyramidal cells, is introduced.
- A soft firing threshold is realized by *voltage-dependent firing probability*.
- Absorbed spikes induce *time-dependent postsynaptic conductance change*, expressed by the alpha-function.

Scaling of the model is unavoidable when it is applied and compared to biological problems of different size. The discretization process of the continuous model ensures that the important quantities be invariant upon scaling. The diffusion terms in the continuous equations of our model incorporate the unequivalent properties of the different neurons of the same type, assuming random processes resulting in minor differences in their behavior. These diffusion phenomena were lost by Ventriglia in the continuous limit and were treated as (in some cases quite significant) numerical errors.

The boundedness of neuronal states is ensured by the ionic currents and the decay of the calcium concentration (see Part I). With the parameters used, very little spontaneous firing occurs due to diffusion.

3 The general population equations

The two main variables of the model are the PDF $g_s(\mathbf{r}, u, \chi, t)$ of neurons and the PDF $f_s^{(\alpha)}(\mathbf{r}, t)$ of spikes. In the following, the time evolution equations of these variables are given. The symbols occurring in the equations below are defined in Appendix A.

3.1 Neurons

The time-evolution equation for the PDF of pyramidal neurons is a balance equation connecting the partial time derivative of g_s, its first partial derivatives with respect to the membrane potential and calcium concentration (i.e. the drift of neurons along these coordinates), and the respective second derivatives (i.e. the diffusion). Thus the left-hand side describes the interspike dynamics while the right-hand side contains a source and a sink term which correspond to neurons returning from firing and those starting to fire, respectively:

$$\begin{aligned}&\frac{\partial g_s(\mathbf{r}, u, \chi, t)}{\partial t} + \frac{\partial}{\partial u}\left(\varepsilon_s(\mathbf{r}, u, \chi, t) \cdot g_s(\mathbf{r}, u, \chi, t)\right) \\ &\quad + \frac{\partial}{\partial \chi}\left(\eta_s(u, \chi) \cdot g_s(\mathbf{r}, u, \chi, t)\right) - \frac{D_u}{2} \cdot \frac{\partial^2 g_s(\mathbf{r}, u, \chi, t)}{\partial u^2} \\ &\quad - \frac{D_\chi}{2} \cdot \frac{\partial^2 g_s(\mathbf{r}, u, \chi, t)}{\partial \chi^2} = b_s(\mathbf{r}, u, \chi, t) - n_s(\mathbf{r}, u, \chi, t) \qquad (1)\end{aligned}$$

where ε_s and η_s describe the electric current and the calcium influx to the cell, respectively, to be specified by the actual single cell model (see Sect. 4). The function n_s

is the PDF expressing the rate with which neurons are starting to fire, and b_s is the same for neurons returning from firing:

$$n_s(\mathbf{r},u,\chi,t) = \begin{cases} p_s(u)\cdot\epsilon_s(\mathbf{r},u,\chi,t)\cdot g_s(\mathbf{r},u,\chi,t) & \text{if } \epsilon_s(\mathbf{r},u,\chi,t)>0 \\ 0 & \text{otherwise} \end{cases} \tag{2}$$

$p_s(u)$ being related to the voltage dependent firing probability (see Part I), and

$$b_s(\mathbf{r},u,\chi,t) = \int_{-\infty}^{t} dt' \int_{-\infty}^{\infty} du' \int_0^{\infty} d\chi' n_s(\mathbf{r},u',\chi',t') \cdot \delta(u-U_s(u',\chi',t'))\cdot\delta(\chi-\chi_s(u',\chi',t'))\cdot\delta(t-T_s(u',\chi',t')) \tag{3}$$

where the functions U_s, χ_s, and T_s contain the firing mechanism, telling when and at which point of the state space the firing should end (see Sect. 4). Equation (3) ensures that the number of neurons is preserved, i.e. after a sufficiently long time, all neurons return from firing.

3.2 Spikes

The time evolution equation for the PDF of spikes is a balance equation connecting the partial time derivative of $f_s^{(\alpha)}$, its space gradient (i.e. the drift of spikes in space), and its Laplaceian (i.e. the diffusion). The right-hand side of the equation is responsible for the absorption and emission of spikes. Absorption is proportional to the number of spikes, i.e. the number of propagating spikes decreases exponentially. Emission of spikes is proportional to the number of firing neurons:

$$\frac{\partial f_{s'}^{(\alpha)}(\mathbf{r},t)}{\partial t} + (\mathbf{v}_{s'}^{(\alpha)}\nabla) f_{s'}^{(\alpha)}(\mathbf{r},t) - \frac{D_r}{2}\cdot\nabla^2 f_{s'}^{(\alpha)}(\mathbf{r},t) = -\sigma_{s'} f_{s'}^{(\alpha)}(\mathbf{r},t) + \lambda_{s'}^{(\alpha)}\cdot\int_{-\infty}^{\infty} du' \int_0^{\infty} d\chi' n_{s'}(\mathbf{r},u',\chi',t) \tag{4}$$

where $\mathbf{v}^{(\alpha)}$ is the velocity of spikes in the direction α, and σ and $\lambda^{(\alpha)}$ are the absorption and emission coefficients, respectively.

3.3 Synapses

The synaptic interaction between neurons takes place when the target population absorbs the spikes emitted by the presynaptic population. First the number of absorbed spikes per neuron should be given:

$$a_{s's}(\mathbf{r},t) = \frac{1}{\phi_s(\mathbf{r})}\cdot w_{s's}\cdot\sigma_{s'}\cdot\int_0^{2\pi} f_{s'}^{(\alpha)}(\mathbf{r},t)\,d\alpha \tag{5}$$

where ϕ_s is the density of neurons at point $\mathbf{r}$, and $w_{s's}$ decides what proportion of the spikes emitted by a neuron of type s' should be absorbed by neurons of type s ($\Sigma_s w_{s's}=1$). Thus the divergence number between the populations s' and s is $\int_0^{2\pi}\lambda_{s'}^{(\alpha)}d\alpha\cdot w_{s's}$. The respective convergence number can be given as $(\phi_{s'}(\mathbf{r})/\phi_s(\mathbf{r}))\cdot\int_0^{2\pi}\lambda_{s'}^{(\alpha)}d\alpha\cdot w_{s's}$.

The postsynaptic conductance is then the integral over past postsynaptic events, all of which are proportional to $a_{s's}$ and are described by the alpha-function:

$$\gamma_{s's}(\mathbf{r},t) = \frac{\bar{\gamma}_{s's}}{\tau_{s's}}\cdot\int_0^{\infty} a_{s's}(\mathbf{r},t-t')\cdot t'\cdot\exp(1-t'/\tau_{s's})\,dt' \tag{6}$$

where $\bar{\gamma}_{s's}$ is the maximal conductance and $\tau_{s's}$ is the time to peak. The postsynaptic conductance is then used in Sect. 4 to determine the postsynaptic current. Thus the interaction between the neural populations is specified.

4 Integrating the single-cell model into the population equations

Three cell types are involved in the model: pyramidal (P) cells, inhibitory cells mediating fast (F) inhibition, and cells mediating slow (S) inhibition. The model for both types of inhibitory (I) cells is a reduction of the pyramidal cell model.

The membrane potential coordinate u and the calcium concentration coordinate χ in the population model stand for the time-dependent variables of the single-cell model, $V(t)$ and $X(t)$, respectively. As Eq. (1) is given for the PDF of neurons, its drift terms correspond to the equations of motion of the single-cell model.

Thus the electric current ε_s in Eq. (1) corresponds to the currents in Part I but consists of not only voltage (and calcium) dependent ionic currents but also the synaptic currents:

$$\varepsilon_s(\mathbf{r},u,\chi,t) = -\frac{1}{C_s}\sum_i I_s^{(i)}(u,\chi) - \frac{1}{C_s}\sum_{s'} I_{s's}^{\mathrm{syn}}(\mathbf{r},u,t) \tag{7}$$

where the ionic currents $I_s^{(i)}$ of different cell types are given in Part I, and C_s is the membrane capacitance of the postsynaptic cell.

4.1 Pyramidal cells

The calcium influx η in Eq. (1) is given in Part I:

$$\eta_{\mathrm{P}}(u,\chi) = -\beta\cdot\chi - B\cdot I_{\mathrm{Ca}}(u) \tag{8}$$

The firing probability $p_{\mathrm{P}}(u)$ in Eq. (2) is the same as $p(V)$ as defined and specified in Part I. The refractoriness and return properties of the neurons can be given by specifying the functions U, χ, and T of Eq. (3). The rather simple case given in Part I can be obtained by setting

$$U_{\mathrm{P}}(u,\chi,t) = V_{\mathrm{ret}}(\chi+\Delta\chi) \tag{9}$$

$$\chi_{\mathrm{P}}(u,\chi,t) = \chi+\Delta\chi \tag{10}$$

$$T_{\mathrm{P}}(u,\chi,t) = t + t^{\mathrm{ref}} \tag{11}$$

where the parameters t^{ref}, $\Delta\chi$, and the function V_{ret} are specified in Part I: Appendix A. The population

framework allows more realistic mechanisms by making use of all three variables of these functions. Now Eq. (3) reduces to

$$b_{\mathrm{P}}(\mathbf{r},u,\chi,t)=\delta(u-V_{\mathrm{ret}}(\chi))\cdot\int_{-\infty}^{\infty}n_{\mathrm{P}}(\mathbf{r},u',\chi-\Delta\chi,t-t^{\mathrm{ref}})\,du' \tag{12}$$

4.2 Inhibitory cells

For inhibitory cells the same kinetics applies but the calcium coordinate does not exist and the number of ionic currents is less (see Part I). For the sake of simplicity, the firing of inhibitory cells is deterministic, and is characterized by the threshold Θ:

$$p_{\mathrm{I}}(u)=\delta(u-\Theta) \tag{13}$$

After firing, the resting potential is restored:

$$U_I(u,t)=E_{\mathrm{rest}} \tag{14}$$

$$T_I(u,t)=t+t^{\mathrm{ref}} \tag{15}$$

4.3 Synapses

For the synaptic current

$$I_{s's}^{\mathrm{syn}}(u,t)=-\gamma_{s's}(\mathbf{r},t)\cdot(u-E_{s's}) \tag{16}$$

where $\gamma_{s's}$ is the synaptic conductance specified in Eq. (6), and $E_{s's}$ is the reversal potential of the synaptic channel.

Four types of synapses are included in the model: (1) pyramidal cell recurrent collateral – pyramidal cell (PP) synapses; (2) fast inhibitory cell – pyramidal cell (FP) synapses; (3) slow inhibitory cell – pyramidal cell (SP) synapses; (4) pyramidal cell – inhibitory cell (both types) (PI) synapses.

5 Discretization and scaling

To run the model in a computer, the above equations should be discretized. The discretization of partial differential equations, however, is nontrivial. The natural requirement is that the discrete equations should approximate the continuous model if the discretization units in all dimensions (including time) tend to zero. Nevertheless, this limit can be very different if the relative rate by which the individual units tend to zero is varied.

We will call the simultaneous change of the discretization units *scaling*. It can be shown that with appropriate *scaling rules* the continuous limit of the discrete equation yields the continuous model and the first two moments of $f_s^{(\alpha)}$ and g_s are *invariant* upon scaling (Appendix B).

From the point of view of discretization, the membrane potential and the calcium coordinates are equivalent and thus a simplified case is studied where the calcium concentration is omitted. For the sake of simplicity, it is also assumed that $\varepsilon_s(\mathbf{r},u,\chi,t)\equiv\epsilon$ is a constant during one time-step.

The discrete time-step Δt is chosen as the single scaling factor which determines all discretization units, according to the requirement that the first two moments of the PDFs should not change for different values of Δt. It can be shown that all discretization units $(\Delta u,\Delta x,\Delta\alpha)$ can be determined for any given value of Δt, preserving the diffusion rates D_u, D_r. The exact form of both PDFs $f_s^{(\alpha)}$ and g_s is calculated in each time step and thus computer simulations can directly be made on the basis of the derived discrete equations. If Δt tends to zero, $\Delta u,\Delta x$, and $\Delta\alpha$ also tend to zero, and the continuous model with diffusion is obtained.

Since neurons are fixed in space, diffusion of g_s only occurs in the coordinate u; on the other hand, diffusion of $f_s^{(\alpha)}$ only occurs in space. Thus these two cases can be discussed separately. The basic idea of distribution into neighboring gridpoints is adopted with the necessary changes from Ventriglia (1988).

6 Results

The role of inhibitory and excitatory interactions is studied in the simulations presented here. A range of epileptiform and non-epileptic rhythms have been obtained. For classification of these behaviors, the measure of synchronization is defined as the percentage of simultaneously (within 3 ms) firing pyramidal cells. The underlying single-cell activities can be studied by collecting the values of synaptic inputs from the simulation of the population model and then running the single-cell model using this data as 'average synaptic input' of the subpopulation containing the given cell. Thus the model also offers the possibility to follow the activity of an 'average cell' at any point of the continuum.

6.1 Temporal phenomena

Computer simulations to study the time-dependent behavior of the model under different conditions were run on a small portion (0.4 mm × 0.4 mm) of the CA3 field. Periodic boundary conditions, however, mimicked an infinite, homogeneous neural space. A small bias current was added to all pyramidal cells as in Traub and Miles (1992), and varied in the different experiments. The values of other parameters are listed in Appendix A. The two types of inhibitory cells receive the same input and thus their behavior is not distinguished (though their effect on pyramidal cells is very different, of course). The figures show the percentage of synchronously firing cells, and the membrane potential of the 'average cell' for both pyramidal and inhibitory cells, and the calcium concentration for pyramidal cells.

First, the synchronized behavior with minimal inhibition ($\gamma_{\mathrm{FP}}=0.01825$ mS cm^{-2}) was studied with a small

bias current ($I_{ext} = 0.09\,\mu A\,cm^{-2}$). The suppression of inhibition leads to synchronized population activity in consequence of the excitatory interactions between pyramidal cells, as comparative experiments and simulations with networks also demonstrate (Traub and Miles 1991, 1992). Minimal inhibition leads to *fully synchronized bursts* (Fig. 1). Bursts occur at 1200 ms intervals. The form of individual bursts with an expressed calcium-spike is shown in the inset. Population synchrony during bursts is close to 100%. Inhibitory cells fire highly synchronous action potentials during pyramidal cell bursts.

Increasing the strength of fast inhibitory synapses, the synchronization of pyramidal cell bursts is gradually abolished. At $\gamma_{FP} = 0.1$ mS cm^{-2}, only a small subpopulation (3%) of pyramidal cells burst; the rest are silent (Fig. 7, top). The frequency of population events slightly increases and they now occur at 900 ms intervals. If the degree of synchronization is low, individual cells very rarely produce a burst, but instead *synchronized synaptic potentials* (SSP) can be observed (Fig. 2, middle). The inset clearly shows the population of excitatory postsynaptic potentials (EPSP) followed by a fast and a slow component of inhibitory postsynaptic potentials (IPSP). Such partially synchronized bursts may correspond to physiological sharp waves in vivo (Traub and Miles 1992). Inhibitory cells show similar synaptic potentials.

Further strengthening of inhibitory connections would abolish pyramidal cell firing (Traub and Miles 1992; Fig. 4/C2). Adding, however, a strong bias current ($I_{ext} = 1.5\,\mu A\,cm^{-2}$) to pyramidal cells, a synchronized subthreshold oscillation emerges with occasional firing (Fig. 3). The frequency of this oscillation (20 Hz) is about 20 times as high as that of SSP. Individual pyramidal cells rarely and irregularly fire and they only fire single action potentials (see inset); no bursts can be found. This phenomenon was also found by Traub and Miles (1992; Fig. 4/A2), and was called 'low amplitude population oscillation'. The number of firing inhibitory cells is much higher (20–40%) and changes irregularly in each period. The inhibitory cell firing-induced fast IPSPs produce the sawtooth-shaped oscillation of pyramidal cells, as already observed by Traub and Miles (1992).

6.2 Spatial patterns

As an illustration of the spatial propagation of activity through the CA3 slice, a 0.4 mm × 1.6 mm slice was

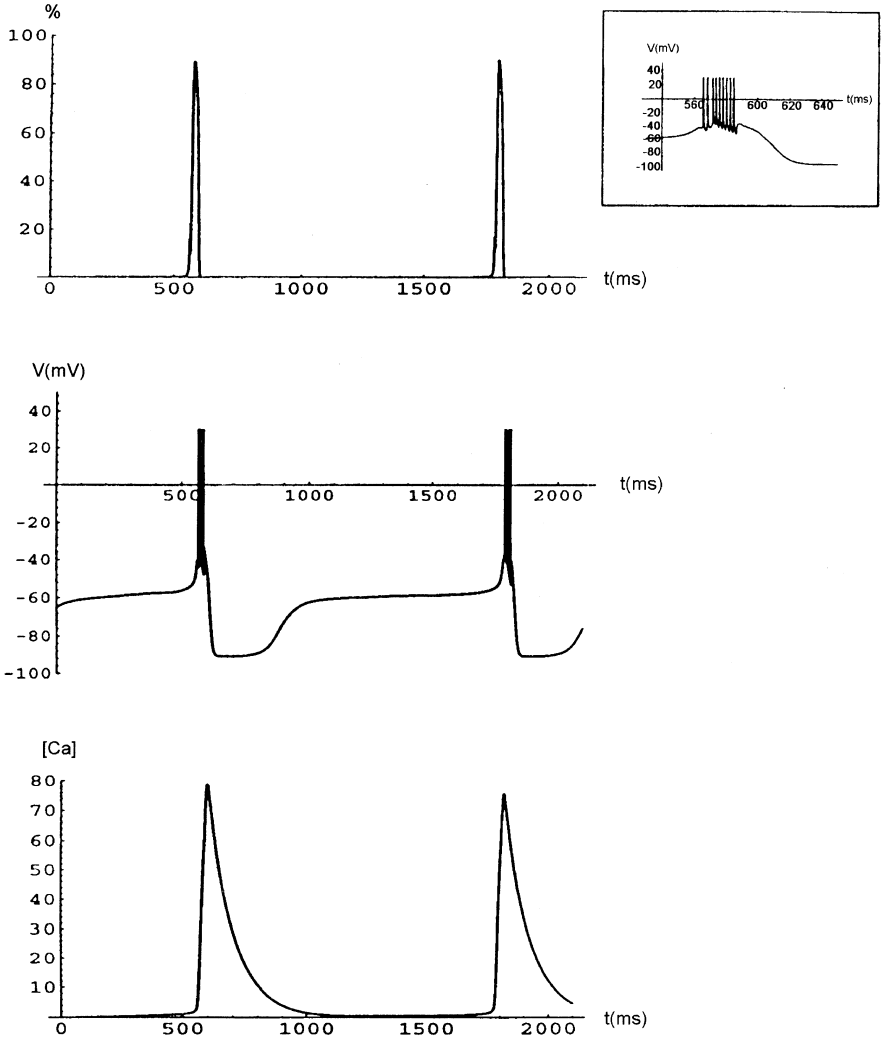

Fig. 1. Fully synchronized population burst ($\gamma_{FP} = 0.01825$ mS cm^{-2}, $I_{ext} = 0.09\,\mu A\,cm^{-2}$): the behavior of pyramidal cells (cf. Traub et al. 1992; Fig. 4/B1). *Top:* percentage of firing cells in the population. *Middle*: membrane potential of an 'average cell'; the burst form is shown in the *inset*. *Bottom*: calcium concentration of the 'average cell'

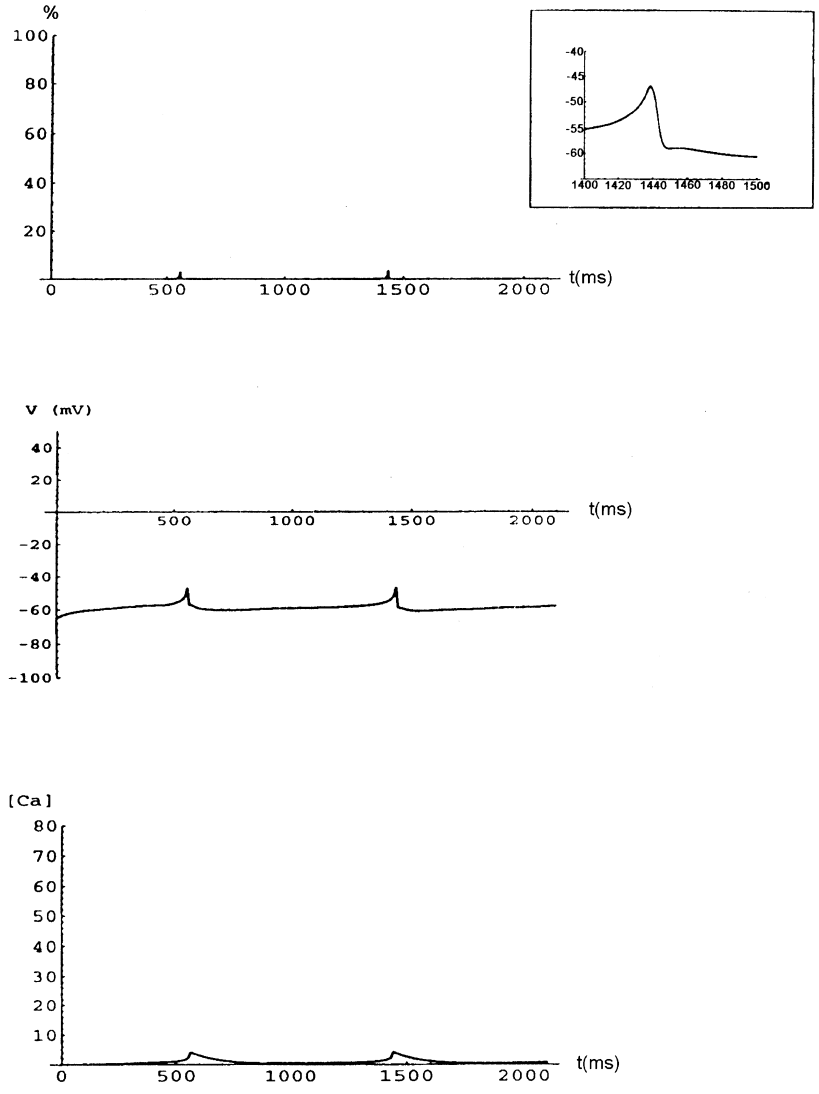

Fig. 2. Synchronized synaptic potentials ($\gamma_{FP} = 0.1$ mS cm^{-2}, $I_{ext} = 0.09\,\mu$A cm^{-2}): the behavior of pyramidal cells (cf. Traub et al. 1992; Fig. 4/C1). *Top*: percentage of firing cells in the population. *Middle*: membrane potential of an 'average cell'; the form of the complex synaptic potential (EPSP, fast IPSP, slow IPSP) is shown in the *inset*. *Bottom*: calcium concentration of the 'average cell'

divided into 8×32 subregions, and a propagating burst without inhibition was observed. The cells in the subregion (5,5) received a strong stimulus through 3 ms. Cells in this subregion developed full burst (Fig. 4, top-left). Burst activity was gradually built up in the neighboring subregions with low propagation velocity (0.033 m s^{-1}). Then bursting of a larger region propagated through the slice with a higher velocity of 0.08 m s^{-1} (see also Fig. 5). Figure 4 shows pairs of 'average cell' membrane potentials (left) and firing percentages (right) of adjacent subregions, spaced 0.2 mm from each other. The inset shows the time of maximal firing as a function of distance from the stimulus. The two fitted lines correspond to the initial and late propagation velocities. Similar results have been obtained by Golomb and Rinzel (1996).

The spatial pattern of propagation can be observed in Figs. 5 and 6. In Fig. 5, a dark color denotes higher percentage of synchronously firing cells, black being 100 percent. The model slice is shown at different times, from top to bottom, first in the left column and then in the right one. The time interval between subsequent frames is 4 ms. A high activity first appears in the stimulated subregion, then builds up in the neighboring regions, and then propagates through the full length of the slice.

In Fig. 6, the membrane potential of the 'average cell' of each subregion is shown. The resting potential is the gray color seen in the first frame. Higher potentials are darker, the firing state being denoted by the black color. Again, subsequent frames are separated by 4 ms intervals. It is interesting to observe that during the quite regular population behavior (Fig. 5), 'average cells' fire irregularly. Light regions in the late frames show the afterhyperpolarization following the burst.

7 Conclusions

In this article we have developed a new theoretical method and a computational model to simulate neural population phenomena, and applied the model to describing the fundamental temporal and spatiotemporal patterns known from hippocampal CA3 slice experiments.

The whole procedure relies on two pillars. The general statistical framework has been developed to treat

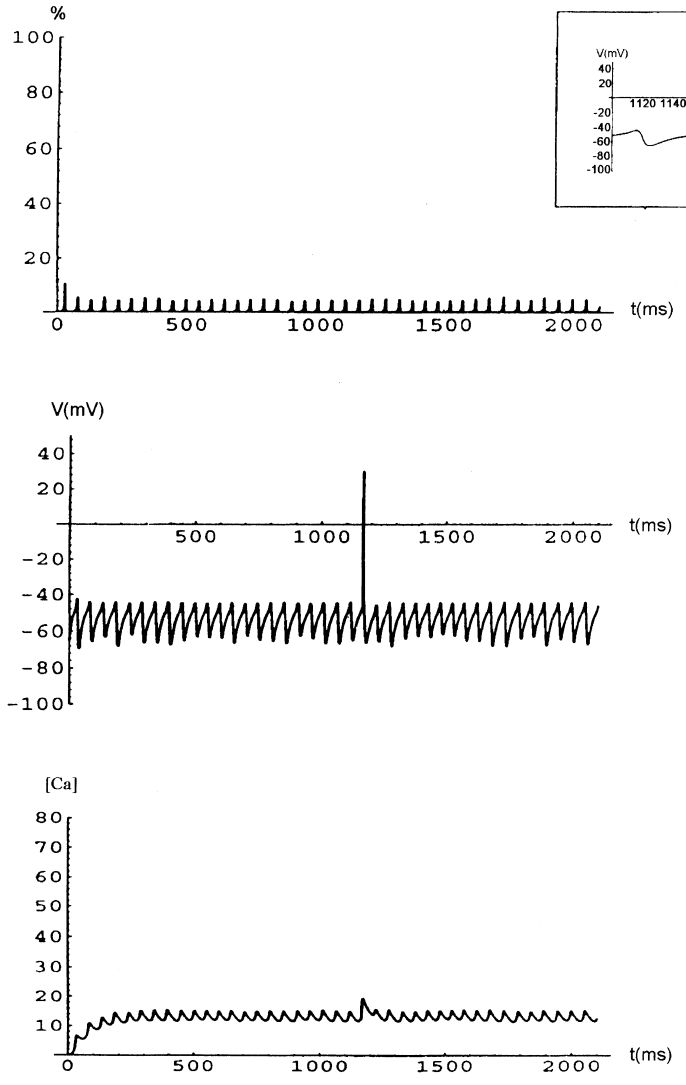

Fig. 3. Low amplitude population oscillation ($\gamma_{FP} = 0.1$ mS cm^{-2}, $I_{ext} = 1.5\,\mu$A cm^{-2}): the behavior of pyramidal cells (cf. Traub et al. 1992; Fig. 4/A2). *Top*: percentage of firing cells in the population. *Middle*: membrane potential of an 'average cell'; the sawtooth shape of the oscillation and a single action potential is shown in the *inset*. *Bottom*: calcium concentration of the 'average cell'

the interaction between large neuronal populations (Part II), and an appropriate single-cell module has been integrated in it (Part I) which made it possible to be applied for a specific brain region, i.e. the CA3 subfield of the hippocampus.

Our statistical theory is motivated by Ventriglia's kinetic theory (Ventriglia 1974, 1988, 1994) and adopts the notion of PDFs of neurons and spikes ('impulses'), but its mathematical apparatus is quite different: in our equations, second derivatives also appear describing diffusion processes. More specifically, the neurons diffuse in the state space and the spikes in the real space. Despite diffusion, however, neurons remain in a bounded region of membrane potential and calcium concentration, owing to the ionic currents and to the decay of calcium concentration, respectively.

The state space is defined by the single-cell model. Since our primary goal is to develop a model for describing hippocampal population activity, the biological plausibility requires that the single-cell model should be sufficently complex to exhibit bursting phenomena. To ensure computational efficiency we sacrificed the multicompartment approach and used single compartments, e.g. as in integrate-and-fire type models. However, in addition to the membrane potential, calcium concentration was also included as a state variable. The details of the action potential generation were neglected. An important methodological advantage of the integration of this single-cell model into the statistical theory is the possibility to simultaneously monitor population and 'average single-cell' behavior.

To illustrate both the correctness and the efficiency of our statistical model, many phenomena, found experimentally in CA3 slices, were simulated. First, it is a fundamental requirement that the basic single-cell firing patterns of the pyramidal cells (measured and simulated with Hodgkin–Huxley technique) should be reproduced. We showed that our model fulfills this requirement. Second, temporal and two-dimensional spatial population phenomena were also simulated. The role of inhibitory and excitatory interactions was studied. A range of epileptiform and non-epileptic rhythms has been obtained. The synaptic strengths of excitatory and inhibitory synapses have been varied. The degree of pyramidal cell synchronization has been studied while it was also possible to monitor single-cell activity underlying

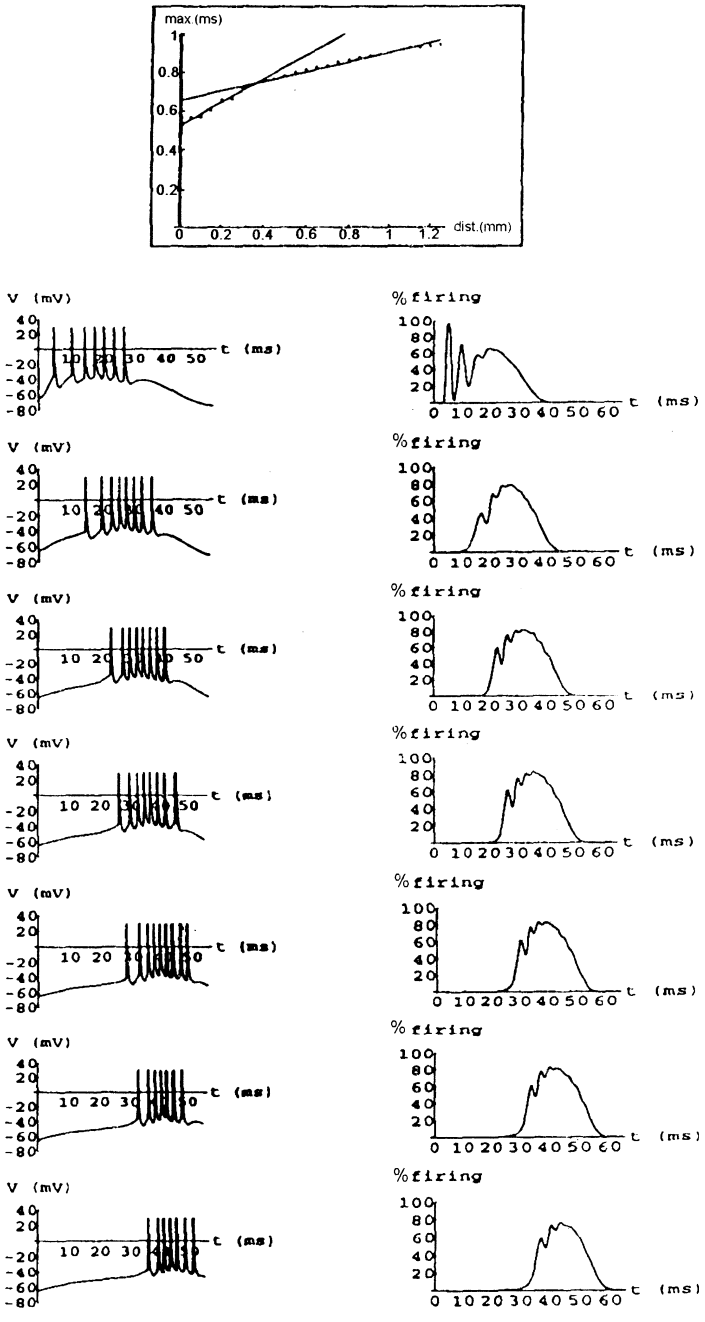

Fig. 4. 'Average cell' membrane potentials (left) and firing percentages (right) of adjacent subregions, spaced 0.2 mm from each other

population behavior. Phenomena that were reproduced included fully synchronized population bursts, synchronized synaptic potentials, and low amplitude population oscillation.

We have now a proper method for treating the dynamics of large-scale neural populations, and have made a first step to apply it to understanding the role of excitatory and inhibitory interactions in hippocampal rhythm generation. There is still a lot to be done. Though our simulations used different levels of inhibition (including the spatial phenomena in the totally disinhibited slice), the systematic study of the model's behavior in terms of the degree of partial inhibition is missing.

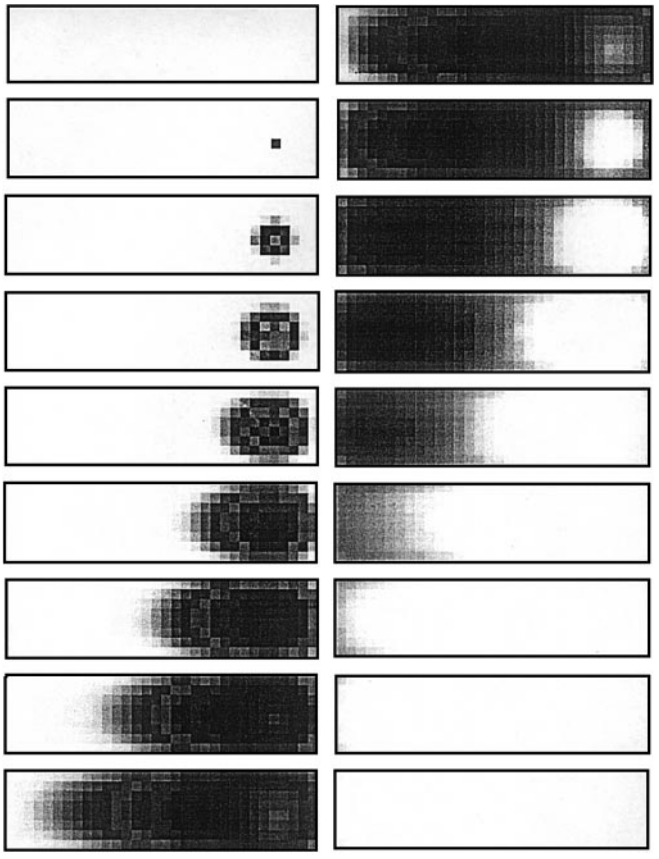

Fig. 5. Percentage of firing pyramidal cells throughout the model slice. Frames (*from top to bottom*, *left column first*) are snapshots after 0, 4, 8, . . . ,68 ms. Dark color denotes high activity

We should turn from slices to in vivo experiments. The scalability of our model enables the simulation of arbitrarily large populations. Our longer term aim is to understand how the hippocampal neural circuitry, supplemented with specific subcortical inputs, can implement different types of dynamic activity ('brain states') such as theta rhythm and sharp waves, and how these activity patterns elicit long term potentiation (LTP) (see also Buzsáki 1989, 1996).

Accordingly, the model can be extended along several lines:

1. Both pyramidal cells and interneurons should receive modulatory input, mimicking different effects of the subcortical innervation. Specifically, periodic input in the theta frequency range could simulate the external source of theta activity. The alternating theta/sharp-wave cycles can then be simulated by regulating the 'subcortical' input.
2. Specific synaptic connections between pyramidal cells can be established as shown by Ventriglia (1988). A major problem to be solved is the scalability of such patch-to-patch connections.
3. Learning phenomena can be studied by incorporating an appropriate learning rule which controls synaptic potentiation (LTP) and depression (LTD).
4. Structured entorhinal input patterns may be used to solve memory tasks characteristic to the hippocampus.

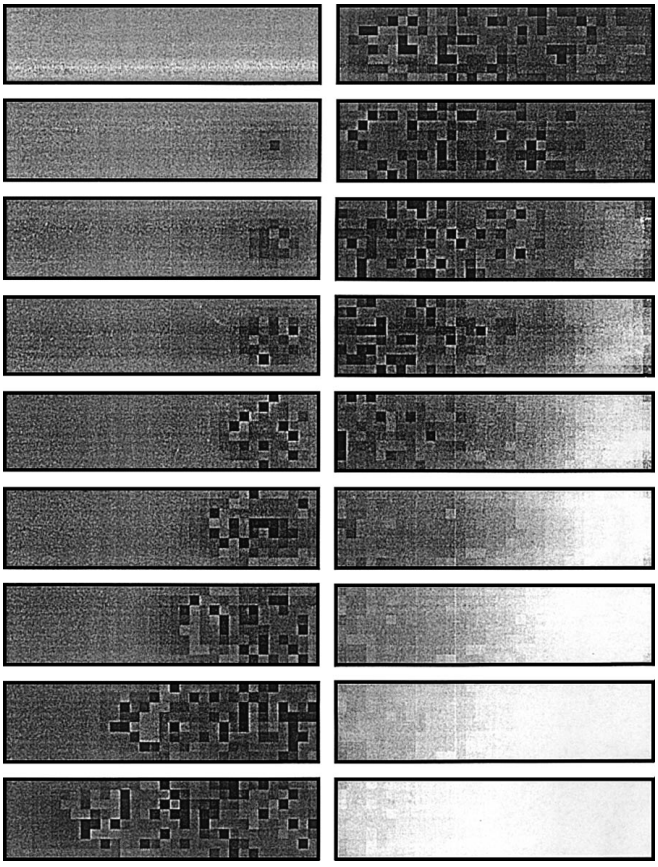

Fig. 6. Membrane potential of the 'average cells' throughout the model slice. Snapshots are taken every 4 ms. *First frame* shows resting potential, *darker colors* correspond to higher potential values. Firing cells are shown in *black*

5. Other regions of the hippocampal formation, such as the entorhinal cortex, the dentate gyrus, CA1, and the subiculum, may be modeled with the same technique, and the cortico-hippocampo-cortical loop can be simulated.
6. The populations of interneurons, and specifically their ability to synchronize oscillation in the gamma frequency range, may also be subject of study.

Acknowledgements. Our work has strongly been motivated by Franceso Ventriglia. We thank the many discussions we had with him in the last 13 years. We also thank Peter Adorján for his invaluable help in the computer implementation. This work was supported by the OTKA grants F014020 and T017784, by the exchange program between the Hungarian Academy of Sciences and the Consiglio Nazionale delle Ricerche (Italy), and by the Fogarty International Research Collaboration Award, HHS Grant No. 1 R03 TW00485-01.

Appendix A. Symbols and parameter values

A.1 State space

Def. 1. $\mathbf{r} = (x, y)$ [mm] is the two-dimensional space coordinate.
Def. 2. u [mV] is the membrane potential coordinate of neurons.
Def. 3. χ [μM] is the intracellular calcium concentration coordinate of neurons.
Def. 4. α [rad] is the angle coordinate of spike propagation.
Def. 5. s is an index referring to different types of neurons: pyramidal cells (P), fast inhibitory cells (F), and slow inhibitory cells (S). Sometimes inhibitory cells are collectively referred to by the index I.

A.2 Neurons

Def. 6. $g_s(\mathbf{r}, u, \chi, t)$ [$\mathrm{mm}^{-2}\ \mathrm{mV}^{-1}\ \mu\mathrm{M}^{-1}$] is the PDF of neurons.
Def. 7. $\phi_s(\mathbf{r})$ [mm^{-2}] is the neuron density at point $\mathbf{r}$. In the simulations, ϕ is homogeneous, and

$$\phi_\mathrm{P}(\mathbf{r}) \equiv 5000\ \mathrm{mm}^{-2}$$

$$\phi_\mathrm{F}(\mathbf{r}) \equiv 200\ \mathrm{mm}^{-2}$$

$$\phi_\mathrm{S}(\mathbf{r}) \equiv 300\ \mathrm{mm}^{-2}$$

Def. 8. $n_s(\mathbf{r}, u, t)$ [$\mathrm{mm}^{-2}\ \mathrm{mV}^{-1}\ \mathrm{ms}^{-1}$] is the PDF of neurons just about to fire.
Def. 9. $b_s(\mathbf{r}, u, t)$ [$\mathrm{mm}^{-2}\ \mathrm{mV}^{-1}\ \mathrm{ms}^{-1}$] is the PDF of neurons returning from firing.
Def. 10. $p_s(u)$ [mV^{-1}] is the probability density of firing.
Def. 11. $\epsilon_s(\mathbf{r}, u, \chi, t)$ [$\mathrm{mV\ ms}^{-1}$] is the net rate of membrane potential change.
Def. 12. $\eta_s(u, \chi)$ [$\mu\mathrm{M\ ms}^{-1}$] is the net rate of calcium concentration change.
Def. 13. D_u [$\mathrm{mV}^2\,\mathrm{ms}^{-1}$] is the diffusion coefficient of neurons along the membrane potential coordinate:

$$D_u = 1\mathrm{m\ V}^2\,\mathrm{ms}^{-1}$$

Def. 14. D_χ [$\mu\mathrm{M}^2\,\mathrm{ms}^{-1}$] is the diffusion coefficient of neurons along the calcium concentration coordinate:

$$D_\chi = 2.5\,\mu\mathrm{M}^2\,\mathrm{ms}^{-1}$$

A.3 Spikes

Def. 15. $f_s^{(\alpha)}(\mathbf{r}, t)$ [$\mathrm{mm}^{-2}\ \mathrm{rad}^{-1}$] is the PDF of spikes moving in the direction α.
Def. 16. $\mathbf{v}_s^{(\alpha)}$ [$\mathrm{mm\ ms}^{-1}$] is the velocity of spike propagation:

$$v_\mathrm{P} = v_\mathrm{I} = 0.5\,\mathrm{mm\,ms}^{-1}$$

Def. 17. $\lambda_s^{(\alpha)}$ [rad^{-1}] is the emission coefficient denoting the number of emitted spikes by a firing neuron in the direction α. The integrated values $\lambda_s = \int_0^{2\pi} \lambda_s^{(\alpha)} d\alpha$ are

$$\lambda_\mathrm{P} = 300$$

$$\lambda_\mathrm{F} = 280$$

$$\lambda_\mathrm{I} = 50$$

Def. 18. σ_s [ms^{-1}] is the absorption rate of spikes:

$$\sigma_\mathrm{P} = 0.35\ \mathrm{ms}^{-1}$$
$$\sigma_\mathrm{I} = 1.75\ \mathrm{ms}^{-1}$$

Def. 19. D_r [$\mathrm{mm}^2\,\mathrm{ms}^{-1}$] is the diffusion coefficient of spikes along the direction of propagation (radial diffusion):

$$D_r = 0.52\ \mathrm{mm}^2\,\mathrm{ms}^{-1}$$

Def. 20. D_t [$\mathrm{mm}^2\,\mathrm{ms}^{-1}$] is the diffusion coefficient of spikes along the direction perpendicular to the propagation (tangential diffusion). In the continuous model $D_t = D_r$.

A.4 Synapses

Def. 21. $a_{s's}(\mathbf{r}, t)$ is the number of absorbed spikes of type s' by a single neuron of type s.

Def. 22. $\gamma_{s's}(\mathbf{r},t)$ [mS cm^{-2}] is the synaptic conductance.

$\gamma_{PP} = 0.003$ mS cm^{-2}

$\gamma_{PI} = 0.004$ mS cm^{-2}

γ_{FP} : varied

$\gamma_{SP} = 0.001$ mS cm^{-2}

Def. 23. $E_{s's}$ [mV] is the synaptic reversal potential:

$E_{PP}(\chi) = -h \cdot \chi \quad h = 1$ mV μM^{-1}

$E_{PI} = -5$ mV

$E_{FP} = -80$ mV

$E_{SP} = -90$ mV

Def. 24. $\tau_{s's}$ [ms] is the time constant of the alpha function:

$\tau_{PP} = 2$ ms

$\tau_{PI} = 0.5$ ms

$\tau_{FP} = 2$ ms

$\tau_{SP} = 30$ ms

Def. 25. $w_{s's}$ is the proportion of absorbed spikes of type s' that are absorbed by the neurons of type s. $\Sigma_s w_{s's} = 1$.

$w_{PP} = 0.933$

$w_{PF} = 0.033$

$w_{PS} = 0.033$

$w_{FP} = 1$

$w_{SP} = 1$

Appendix B. The discretization method

B.1 Discretization in time

B.1.1 Neurons

For the sake of simplicity, the discretization method is demonstrated for the following simplified neuronal equation:

$$\frac{\partial g(\mathbf{r},u,t)}{\partial t} + \epsilon\frac{\partial g(\mathbf{r},u,t)}{\partial u} - \frac{D_u}{2}\cdot\frac{\partial^2 g(\mathbf{r},u,t)}{\partial u^2} = b(\mathbf{r},u,t) - n(\mathbf{r},u,t) \tag{17}$$

The complete equation has been discretized in a similar way.

The discrete difference equation can be obtained by solving Eq. (17) in the time interval $(t, t+\Delta t)$. Since the time step Δt is much smaller than the refractory period t^{ref}, b can be regarded as an external term, and the equation can be solved without b, only adding b after the time step has been completed. Then using Eq. (2), the solution becomes

$$g(\mathbf{r},u,t+\Delta t) = \int_{-\infty}^{\infty} g(\mathbf{r},u',t)\cdot\mathscr{G}(u-(u'+\epsilon\Delta t),\Delta t)\cdot(1-P(u',u))\,du' \tag{18}$$

where $\mathscr{G}$ is the Gaussian $\mathscr{G}(u,t) = 1/(\sqrt{2\pi}D_u t)\cdot\exp(-u^2/2D_u t)$ and

$$P(u_1,u_2) = \begin{cases} 1-\exp(-\int_{u_1}^{u_2} p(u'')\,du'') & \text{if } u_1 < u_2 \\ 0 & \text{otherwise} \end{cases} \tag{19}$$

Because of the requirement of scalability, it is important to note that the solution of Eq. (18) has the property that two consecutive time steps can exactly be replaced with a single, longer time step.

For the number of firing cells in $(t, t+\Delta t)$,

$$N(\mathbf{r},u,t) = \int_t^{t+\Delta t} n(\mathbf{r},u,t')\,dt' = \int_{-\infty}^{\infty} g(\mathbf{r},u',t)\cdot\mathscr{G}(u-(u'+\epsilon\Delta t),\Delta t)\cdot P(u',u)\,du' \tag{20}$$

The amount of returning cells to be added to g is then

$$B(\mathbf{r},u,t) = \delta(u-V_{\text{ret}})\cdot\int_{-\infty}^{\infty} N(\mathbf{r},u',t-t^{\text{ref}})\,du' \tag{21}$$

just as in Eq. (12).

B.1.2. Spikes

The discrete difference equation for spikes can be obtained by solving the linear Eq. (4) in the interval $(t, t+\Delta t)$:

$$f^{(\alpha)}(\mathbf{r},t+\Delta t) = \exp(-\sigma\Delta t)\cdot\int d^2r'\mathscr{G}_r(\mathbf{r}-(\mathbf{r}'+\mathbf{v}^{(\alpha)}\Delta t),\Delta t)f^{(\alpha)}(\mathbf{r}',t) + \lambda^{(\alpha)}\int_{-\infty}^{\infty} N(\mathbf{r},u',t)\,du' \tag{22}$$

where $\mathscr{G}_r(\mathbf{r},t) = 1/2\pi D_r t\cdot\exp(-r^2/2D_r t)$ is the two-dimensional Gaussian.

B.1.3 Synapses

To discretize Eq. (6), we make use of the property of the alpha function $\alpha(t) = (\bar{\gamma}/\tau)\cdot t\cdot\exp(1-t/\tau)$ that it is the solution of the following second-order differential equation:

$$\alpha(t) + 2\tau\frac{d\alpha(t)}{dt} + \tau^2\frac{d^2\alpha(t)}{dt^2} = 0 \tag{23}$$

This second-order differential equation can be written in the form of two first-order differential equations:

$$\frac{d\alpha_0(t)}{dt} = \alpha_1(t)$$
$$\frac{d\alpha_1(t)}{dt} = -\frac{1}{\tau^2}\alpha_0(t) - \frac{2}{\tau}\alpha_1(t) \tag{24}$$

with

$$\alpha_0(0) = 0$$
$$\alpha_1(0) = \frac{\bar{\gamma}}{\tau}\cdot\mathrm{e} \tag{25}$$

Eq. (24) can be discretized as

$$\alpha_0(t+\Delta t) = \alpha_0(t) + \Delta t\cdot\alpha_1(t)$$

$$\alpha_1(t+\Delta t) = -\frac{\Delta t}{\tau^2}\cdot\alpha_0(t) + \left(1-\frac{2\Delta t}{\tau}\right)\cdot\alpha_1(t) \tag{26}$$

Similarly, Eq. (6) can be discretized by introducing two variables γ_0 ($\equiv\gamma$) and γ_1, and by changing the integration variable:

$$\gamma_0(\mathbf{r},t) = \int_{-\infty}^{t} a(\mathbf{r},t')\cdot\alpha_0(t-t')\,dt'$$
$$\gamma_1(\mathbf{r},t) = \int_{-\infty}^{t} a(\mathbf{r},t')\cdot\alpha_1(t-t')\,dt' \tag{27}$$

Now we obtain (by changing the integration variable again)

$$\begin{aligned}\gamma_0(\mathbf{r},t+\Delta t) &= \gamma_0(\mathbf{r},t)+\Delta t\cdot\gamma_1(\mathbf{r},t)+\int_0^{\Delta t} a(\mathbf{r},t+\Delta t-t'')\cdot\alpha_0(t'')\,dt''\\ \gamma_1(\mathbf{r},t+\Delta t) &= -\frac{\Delta t}{\tau^2}\cdot\gamma_0(\mathbf{r},t)+\left(1-\frac{2\Delta t}{\tau}\right)\cdot\gamma_1(\mathbf{r},t)\\ &\quad+\int_0^{\Delta t} a(\mathbf{r},t+\Delta t-t'')\cdot\alpha_1(t'')\,dt'' \end{aligned} \tag{28}$$

Now if we expand α_0 in Taylor series, the leading term will be $\alpha_0(0)=0$, and the other terms, after integration, will be of order $(\Delta t)^2$. On the other hand, the leading term of α_1 is $\alpha_1(0)=\bar{\gamma}/\tau\cdot\mathrm{e}$, so we obtain:

$$\begin{aligned}\gamma_0(\mathbf{r},t+\Delta t) &= \gamma_0(\mathbf{r},t)+\Delta t\cdot\gamma_1(\mathbf{r},t)\\ \gamma_1(\mathbf{r},t+\Delta t) &= -\frac{\Delta t}{\tau^2}\cdot\gamma_0(\mathbf{r},t)+(1-\frac{2\Delta t}{\tau})\cdot\gamma_1(\mathbf{r},t)+\bar{\gamma}/\tau\cdot\mathrm{e}\cdot A(\mathbf{r},t)\end{aligned} \tag{29}$$

where $A(\mathbf{r},t)=\int_t^{t+\Delta t} a(\mathbf{r},t')\,dt'$ can easily be obtained from Eq. (5), assuming that in the discrete model f is constant between t and $t+\Delta t$:

$$A(\mathbf{r},t)=\frac{1}{\phi(\mathbf{r})}\cdot w\cdot\sigma\cdot\Delta t\cdot\int_0^{2\pi} f^{(\alpha)}(\mathbf{r},t)d\alpha \tag{30}$$

Thus Eq. (29) yields the updating rule of the synaptic conductances.

B.2. Discretization of the state space

B.2.1 Neurons

Let the function g be restricted to the equidistant gridpoints of the state space

$$\begin{aligned}x_i &= i\cdot\Delta x\\ y_j &= j\cdot\Delta x\\ u_k &= k\cdot\Delta u\end{aligned} \tag{31}$$

Then

$$g(x,y,u,t)=\sum_{i,j,k=-\infty}^{\infty} G_{ijk}(t)\cdot\delta(x-x_i)\cdot\delta(y-y_j)\cdot\delta(u-u_k) \tag{32}$$

Now Eq. (18) becomes

$$\begin{aligned}g(\mathbf{r},u,t+\Delta t) &= \sum_{i,j=-\infty}^{\infty}\delta(x-x_i)\cdot\delta(y-y_j)\\ &\quad\cdot\sum_{k=-\infty}^{\infty} G_{ijk}(t)\cdot\mathscr{G}(u-(u_k+\epsilon\Delta t),\Delta t)\cdot(1-P(u_k,u))\end{aligned} \tag{33}$$

The key step is the discretization of the Gaussian $\mathscr{G}(u-(u_k+\varepsilon\Delta t),\Delta t)$. We want to determine the minimal number of gridpoints into which the Gaussian can be distributed, preserving both its first and second moments. Let $\mathscr{G}$ be restricted into two neighboring gridpoints

$$\begin{aligned}\mathscr{G}_u(u-(u_l+r\Delta u),\Delta t) &\approx (1-r)\cdot\delta(u-u_l)\\ &\quad+r\cdot\delta(u-u_{l+1})\end{aligned} \tag{34}$$

It is easy to see that this approximation preserves the first moment $(u_k+r\Delta u)$ and it can be shown that (the expected value of) the second moment $(D_u\Delta t)$ is also preserved if r is a random number of uniform distribution in (0,1) and the first scaling rule

$$\Delta u=\sqrt{6D_u\Delta t} \tag{35}$$

holds.

In Eq. (33), the role of r is played by the part of $\epsilon\Delta t$ that falls between two gridpoints, i.e.

$$r=\{\mathscr{E}\},\quad \mathscr{E}=\frac{\epsilon\Delta t}{\Delta u} \tag{36}$$

$\{\ \}$ denoting the fraction part. To make sure that $\{\mathscr{E}\}$ follows a uniform distribution from time-step to time-step (which is a good approximation if $\epsilon\Delta t\gg\Delta u$), the grid itself is moved by a random fraction of Δu in each time-step. The index l in Eq. (34) stands for $k+[\mathscr{E}]$ where [ ] denotes the integer part.

Now substituting Eq. (34) into Eq. (33) and using Eq. (32) to the l.h.s. we obtain the equation of motion for G_{ijk}:

$$\begin{aligned}G_{ijk}(t+\Delta t) &= (1-\{\mathscr{E}\})\cdot(1-P(u_{k-[\mathscr{E}]},u_k))\cdot G_{ij,k-[\mathscr{E}]}(t)\\ &\quad+\{\mathscr{E}\}\cdot(1-P(u_{k-[\mathscr{E}]-1},u_k))\cdot G_{ij,k-[\mathscr{E}]-1}(t)\end{aligned} \tag{37}$$

Similarly, for the number of firing cells

$$\begin{aligned}N_{ijk}(t) &= (1-\{\mathscr{E}\})\cdot P(u_{k-[\mathscr{E}]},u_k)\cdot G_{ij,k-[\mathscr{E}]}(t)\\ &\quad+\{\mathscr{E}\}\cdot P(u_{k-[\mathscr{E}]-1},u_k)\cdot G_{ij,k-[\mathscr{E}]-1}(t)\end{aligned} \tag{38}$$

and the number of returning cells to be added to G_{ijk} in each time step is

$$B_{ijk}(t)=\delta_{kk_{\mathrm{ret}}}\cdot\sum_{k'=-\infty}^{\infty} N_{ijk'}(t-t^{\mathrm{ref}}) \tag{39}$$

as in Eq. (21) where δ is the Kronecker delta and $u_{k_{\mathrm{ret}}}=V_{\mathrm{ret}}$.

B.2.2 Spikes

Again, let

$$\begin{aligned}f_s^{(\alpha)}(\mathbf{r},t) &= \sum_{i,j=-\infty}^{\infty}\sum_{m=1}^{2\pi/(\Delta\alpha)} F_{ijm}(t)\\ &\quad\cdot\delta(x-x_i)\cdot\delta(y-y_j)\cdot\delta(\alpha-\alpha_m)\end{aligned} \tag{40}$$

Then Eq. (22) becomes

$$\begin{aligned}f^{(\alpha)}(\mathbf{r},t+\Delta t) &= \mathrm{e}^{-\sigma\Delta t}\cdot\sum_{i,j=-\infty}^{\infty}\sum_{m=1}^{2\pi/(\Delta\alpha)}\delta(\alpha-\alpha_m)\\ &\quad\cdot\Big(F_{ijm}(t)\cdot\mathscr{G}_r(\mathbf{r}-(\mathbf{r}_{ij}+\mathbf{v}^{(\alpha)}\Delta t),\Delta t)\\ &\quad+\delta(x-x_i)\cdot\delta(y-y_j)\cdot\sum_{k'=-\infty}^{\infty}\lambda_m N_{ijk'}(t)\Big)\end{aligned} \tag{41}$$

Again, the Gaussian should be discretized by being restricted to the minimal number of gridpoints of the two-dimensional lattice. This is more difficult than in the one-dimensional case since the number of possibilities is much larger. It seems to be a plausible solution to distribute the Gaussian into the four corners of the square in which its center is. It can, however, be shown that in this case for a given diffusion rate, Δx has a nonzero lower bound when $\Delta t=0$ and the division cannot be further refined, violating the requirement of scaling invariance.

It was found that the simplest case in which scaling invariance can be achieved is when the distribution is into five points like a cross (Fig. 7). Thus the Gaussian $\mathscr{G}_r$ of Eq. (41) can be approximated by

$$\begin{aligned}\mathscr{G}_r(\mathbf{r}-(\mathbf{r}_{ij}+\mathbf{v}^{(\alpha)}\Delta t),\Delta t) &\approx \rho_0\cdot\delta(x-x_i)\cdot\delta(y-y_j)\\ &\quad+\rho_{+x}\cdot\delta(x-x_{i+1})\cdot\delta(y-y_j)\\ &\quad+\rho_{+y}\cdot\delta(x-x_i)\cdot\delta(y-y_{j+1})\\ &\quad+\rho_{-x}\cdot\delta(x-x_{i-1})\cdot\delta(y-y_j)\\ &\quad+\rho_{-y}\cdot\delta(x-x_i)\cdot\delta(y-y_{j-1})\end{aligned} \tag{42}$$

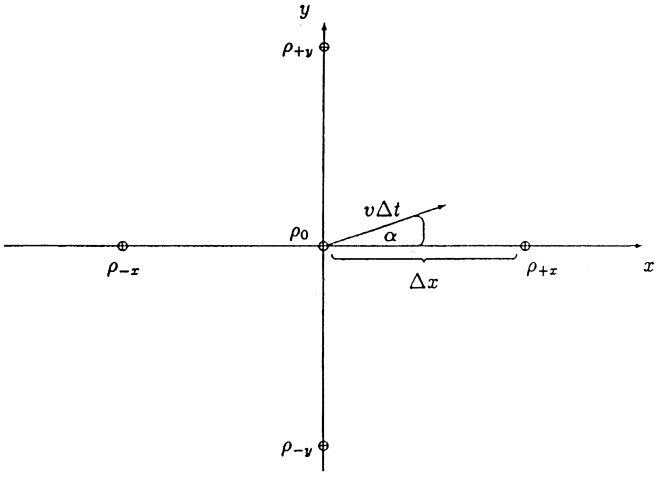

Fig. 7. Approximation of a Gaussian, centered at the arrowhead, with five gridpoints. The fractions ρ_0, ρ_{+y}, ρ_{+x}, ρ_{-y}, ρ_{-x} are distributed into the points indicated with the circles at the *center*, *top*, *right*, *bottom*, and *left*, respectively

which yields the time evolution equation for F_{ijm}:

$$\begin{aligned} F_{i,j,m}(t+\Delta t) = \mathrm{e}^{-\sigma_s \Delta t} \cdot \Big(& \rho_0 \cdot F_{i,j,m}(t) \\ & + \rho_{+x} \cdot F_{i-1,j,m}(t) + \rho_{+y} \cdot F_{i,j-1,m}(t) \\ & + \rho_{-x} \cdot F_{i+1,j,m}(t) + \rho_{-y} \cdot F_{i,j+1,m}(t) \Big) \\ & + \Sigma_{k'=-\infty}^{\infty} \lambda_m N_{ijk'}(t) \end{aligned} \tag{43}$$

Now we require that the first moment of the approximation be $\mathbf{r}_{ij} + \mathbf{v}^{(\alpha)}\Delta t$. For the second moment the following should be noted: although in Eq. (4) a single diffusion coefficient D_r is given for the sake of simplicity, it is not necessary that the diffusion rate along the two coordinate be the same. Now for each direction α_m we decompose the diffusion rate into a component in this direction (radial diffusion, D_r) and another component perpendicular to this direction (tangential diffusion, D_t). To obtain the coefficients ρ of Eq. (42) we only require that the radial component of the second moment be $D_r\Delta t$. The role of D_t is discussed later.

If $0 \le \rho_0 < 1$ is chosen arbitrarily and is independent of α (which is suggested by the symmetry of the arrangement), then the only solution that ensures that the radial variance is independent of α is:

$$\begin{aligned} \rho_{+x} &= \frac{1-\rho_0}{4} + \frac{v\Delta t}{2\Delta x} \cdot \cos\alpha \\ \rho_{+y} &= \frac{1-\rho_0}{4} + \frac{v\Delta t}{2\Delta x} \cdot \sin\alpha \\ \rho_{-x} &= \frac{1-\rho_0}{4} - \frac{v\Delta t}{2\Delta x} \cdot \cos\alpha \\ \rho_{-y} &= \frac{1-\rho_0}{4} - \frac{v\Delta t}{2\Delta x} \cdot \sin\alpha \end{aligned} \tag{44}$$

then the first moment is obviously correct and the condition for the scaling invariance of D_r is:

$$\Delta x = \sqrt{\frac{2\Delta t(v^2\Delta t + D_r)}{1-\rho_0}} \tag{45}$$

which is the second scaling rule.

To ensure that all coefficients ρ fall in the interval (0,1), an additional inequality must hold:

$$\Delta t < \frac{1-\rho_0}{1+\rho_0} \cdot \frac{1}{v^2} \cdot D_r \tag{46}$$

Inequality (46) shows that the economy of computation prefers ρ_0 being close to zero. To determine the free parameter ρ_0, however, another requirement can also be made: it is easy to see that the other four points of the distribution lie in a plane which is $(1-\rho_0)/4$ above the origin. In order to avoid a 'hole' in the distribution, it is required that the central point ρ_0 be above this plane which can be fulfilled by

$$\rho_0 \ge 1/5. \tag{47}$$

The distribution rule (44) also implies that

$$D_t = D_r + v^2\Delta t \tag{48}$$

which is not scaling invariant. Nevertheless, D_t is just the tangential diffusion rate for ***one direction***. The role of tangential diffusion is to fill the gap between neighboring directions. Thus it is enough to ensure that the angle difference $\Delta\alpha$ be smaller than some value determined by D_t. Other considerations suggest the following scaling rule for $\Delta\alpha$:

$$\tan\frac{\Delta\alpha}{2} = c \cdot \sqrt{\frac{v^2\Delta t}{D_r}} \tag{49}$$

with the constant c adjusted to the number of directions when Δt is maximal. Since $2\pi/\Delta\alpha$ must be an integer, Δt and all the other discretization units can only have discrete values. Choosing an appropriately small value for c, however, the neighboring discrete values will be sufficiently close.

B.2.3 Synapses

The equation for postsynaptic conductances in the gridpoints is the same as in the continuous equation (Eq. 29):

$$\begin{aligned} \gamma_{0,ij}(t+\Delta t) &= \gamma_{0,ij}(t) + \Delta t \cdot \gamma_{1,ij}(t) \\ \gamma_{1,ij}(t+\Delta t) &= -\frac{\Delta t}{\tau^2} \cdot \gamma_{0,ij}(t) + \left(1 - \frac{2\Delta t}{\tau}\right) \cdot \gamma_{1,ij}(t) \\ &\quad + \bar{\gamma}/\tau \cdot \mathrm{e} \cdot A_{ij}(t) \end{aligned} \tag{50}$$

where

$$A_{ij}(t) = \frac{1}{\Phi_{ij}} \cdot w \cdot \sigma \cdot \Delta t \cdot \sum_{m=1}^{2\pi/(\Delta\alpha)} F_{ijm}(t) \tag{51}$$

where Φ_{ij} is the number of neurons in the gridpoint (i,j).

References

Amari S (1974) A method of statistical neurodynamics. Kybernetik 14:201–25

Amari S (1983) Field theory of self-organizing neural nets. IEEE Trans SMC 13:741–748

Beurle RL (1956) Properties of a mass of cells capable of regenerating pulses. Phil Trans R Soc 204A:55–94

Buzsáki G (1989) Two-stage model of memory trace formation: A role for 'noisy' brain states. Neuroscience 31:551–570

Buzsáki G (1996) The hippocampo-neocortical dialogue. Cereb Cortex 6:81–92

Cowan J (1968) Statistical mechanics of neural nets. In: Caianiello E (ed) Neural networks. Springer, Berlin Heidelberg New York, pp 181–188

Érdi P, Aradi, I, Grőbler T (1997) Rhythmogenesis in single cell and population models: olfactory bulb and hippocampus. BioSystems 40:45–53

Golomb D, Rinzel J (1996) Minimal biophysical models of oscillations and waves in thalamus and hippocampus. In: Reggia J,

Ruppin E, Sloan Berndt R, (eds) Neural modeling of brain and cognitive disorders. World Scientific, Singapore, pp 327–346
Griffith JA (1963) A field theory of neural nets. I. Derivation of field equations. Bull Math Biophys 25:111–120
Grőbler T, Barna G (1996) A statistical model of the CA3 region of the hippocampus. In: Trappl R (ed) Cybernetics and systems '96, Austrian Society for Cybernetic Studies, Vienna, pp 503–507
Grőbler T, Barna G (1997) Single cell and population activity in a statistical model of the hippocampal CA3 region. In: Bower JM (ed) Computational neuroscience (CNS '96). Plenum, New York, B
Ingber L (1982) Statistical mechanics of neocortical interactions. I. Basic formulation. Physica 5D:83–107
Mallot H, Giannakopoulos F (1996) Population networks: a large-scale framework for modelling cortical neural networks. Biol Cybern 75:441–452
Peretto P (1984) Collective properties of neural networks: a statistical approach. Biol. Cybern. 50:51–62
Peretto P (1992) An Introduction to the Modeling of Neural Networks. Cambridge University Press, Cambridge
Seelen W von (1968) Informationsverarbeitung in homogenen Netzen von Neuronenmodellen. Kybernetik 5:181–194
Traub RD, Miles R (1991) Neuronal networks of the hippocampus. Cambridge University Press, New York
Traub RD, Miles R (1992) Modeling hippocampal circuitry using data from whole cell patch clamp and dual intracellular recordings in vitro. Seminars Neurosci 4:27–36
Ventriglia F (1974) Kinetic approach to neural systems. I. Bull Math Biol 36:534–544
Ventriglia F (1988) Computational simulation of activity of cortical-like neural systems. Bull Math Biol 50:143–185
Ventriglia F (1990) Activity in cortical-like neural systems: short-range effects and attention phenomena. Bull Math Biol 52:397–429
Ventriglia F (1994) Towards a kinetic theory of cortical-like neural fields. In: Ventriglia F (ed) Neural modeling and neural networks. Pergamon Press, Oxford, pp 217–249
Wilson HR, Cowan JD (1973) A mathematical theory of functional dynamics of cortical and thalamic nervous tissue. Kybernetik 13:55–80